Soft Matter

ARTICLE TYPE

Cite this: DOI: 00.0000/xxxxxxxxxx

Supplementary Information: A Dynamical System Approach to Relaxation in Glass-Forming Liquids†

Jack F. Douglas,*[a] Qi-Lu Yuan,[b,c] Jiarui Zhang,[d] Hao Zhang,*[d] and Wen-Sheng Xu*[b,c]

S1 Fit Parameters Related to the Specific Energy and Mean Squared Interparticle Spacing

Here, we provide the fit parameters $\varepsilon_{s,0}$ and ε_s^* utilized in constructing Fig. 1 in the main text regarding the relation between ε_s and $\langle u^2\rangle/k_BT$. Fig. S1 and Table S1 summarize the results for polymer melts and metallic glasses, respectively. Note that ε_s is positive in polymer melts, while this quantity is negative in metallic glasses, so the sign of $\varepsilon_{s,0}$ is different in these two types of models. In addition, we provide the fit parameters a and b utilized in constructing Fig. 2 in the main text regarding the relation between q_p and k_BT. Fig. S2 and Table S2 summarize the results for polymer melts and metallic glasses, respectively.

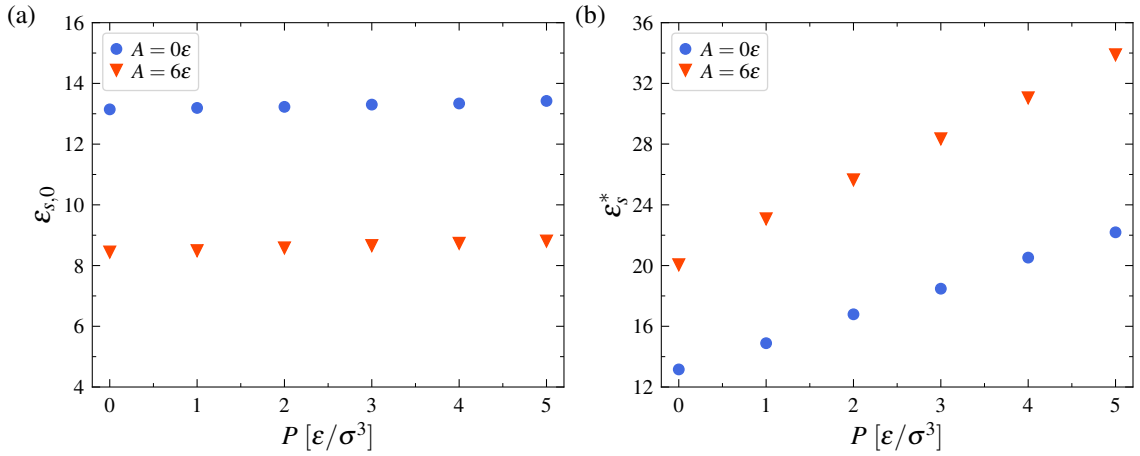

Fig. S1 Fit parameters $\varepsilon_{s,0}$ and ε_s^* as a function of P utilized in constructing Fig. 1a and 1b in the main text for the relation between ε_s and $\langle u^2\rangle/k_BT$. Panels (a) and (b) correspond to the results of both flexible and semi-flexible polymer melts for $\varepsilon_{s,0}$ and ε_s^*, respectively.

Table S1 Fit parameters $\varepsilon_{s,0}$ and ε_s^* utilized in constructing Fig. 1c in the main text for the relation between ε_s and $\langle u^2\rangle/k_BT$ for representative metallic glasses.

MGs	$Cu_{64}Zr_{36}$	$Cu_{36}Zr_{64}$	$Cu_{50}Zr_{50}$	$Ni_{50}Nb_{50}$	$Ni_{62}Nb_{38}$	$Pd_{82}Si_{18}$
$\varepsilon_{s,0}$	−4.29	−5.20	−4.75	−5.90	−5.62	−4.33
ε_s^*	0.27	0.31	0.27	0.43	0.46	0.24

Table S2 Fit parameters a and b utilized in constructing Fig. 2c in the main text for the relation describing the mean squared interparticle spacing parameter q_p^2 over a range of T for representative metallic glasses.

MGs	$Cu_{64}Zr_{36}$	$Cu_{36}Zr_{64}$	$Cu_{50}Zr_{50}$	$Ni_{50}Nb_{50}$	$Ni_{62}Nb_{38}$	$Pd_{82}Si_{18}$
a	58.09	49.31	45.61	51.98	54.32	49.18
b	0.76	10.32	14.90	5.56	6.79	12.81

[a] Materials Science and Engineering Division, National Institute of Standards and Technology, Gaithersburg, Maryland 20899, United States. E-mail: jack.douglas@nist.gov
[b] State Key Laboratory of Polymer Physics and Chemistry, Changchun Institute of Applied Chemistry, Chinese Academy of Sciences, Changchun 130022, P. R. China. E-mail: wsxu@ciac.ac.cn
[c] School of Applied Chemistry and Engineering, University of Science and Technology of China, Hefei 230026, P. R. China.
[d] Department of Chemical and Materials Engineering, University of Alberta, Edmonton, Alberta T6G 1H9, Canada. E-mail: hao7@ualberta.ca

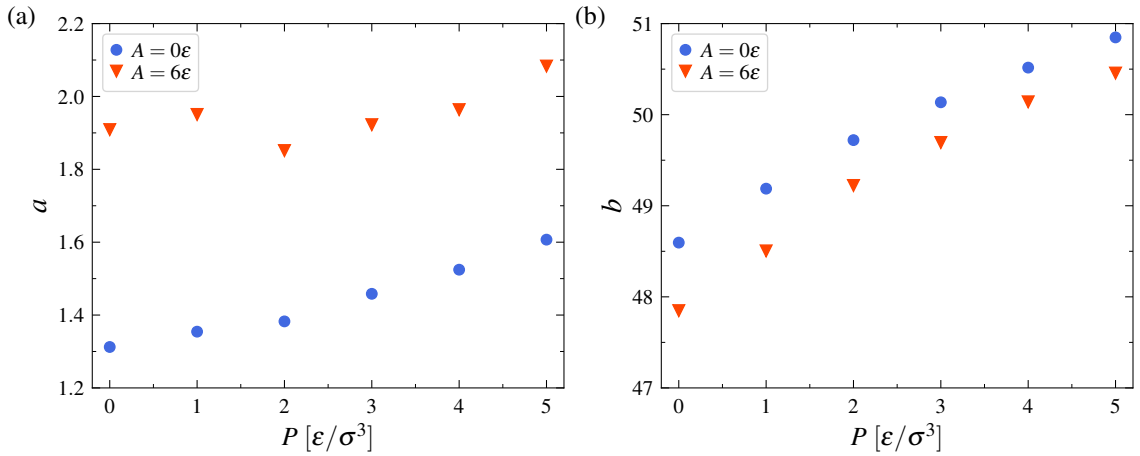

Fig. S2 Fit parameters a and b utilized in constructing Fig. 2a and 2b in the main text for the relation describing the mean squared interparticle spacing q_p^2 over a range of T for polymer melts. Panels (a) and (b) correspond to the results of both flexible and semi-flexible polymer melts for a and b, respectively.

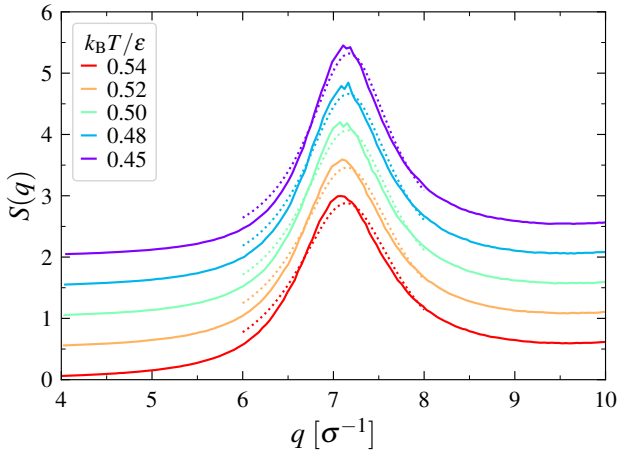

Fig. S3 Static structure factor $S(q)$ of flexible polymer melts for a range of T at $P = 0.0\varepsilon/\sigma^3$. The dotted lines are the fitted results according to the Lorentz equation (Eq. 1). The results at lower T are shifted up by 0.5 from the preceding one.

We also discuss the T dependence of the primary peak position q_p of $S(q)$ in greater detail. In the case of the polymer melt data, we estimate q_p more accurately by fitting the simulation data for $S(q)$ to the Lorentz equation,

$$S(q) = D\left[\frac{C}{(q-q_p)^2 + C^2}\right] \tag{1}$$

where D and C are the additional fitting parameters. The fits were performed in the range of $6\sigma^{-1} < q < 9\sigma^{-1}$, since q_p is found to be generally about $7\sigma^{-1}$ in our polymer model. Fig. S3 shows the $S(q)$ of flexible polymer melts for a range of T at $P = 0.0\varepsilon/\sigma^3$, along with the fitted results. As can be seen, Eq. 1 provides a satisfactory description of $S(q)$ in the q range near q_p.

We note that the T dependence of q_p^2 under constant density conditions is normally quite distinct from the material under constant P conditions. Fig. S4 shows q_p^2 for the 32-atom single-component LJ liquid over a wide range of T at $\rho = 1.0\sigma^{-3}$, where it is evident that q_p^2 has virtually no T dependence. Fig. S5 compares q_p^2 under constant P and ρ conditions for the Kob-Andersen model as a further illustration of the distinct T dependence of q_p^2 under adiabatic and isobaric conditions for the same GF liquid. Overall, the general trends in the T dependence of q_p^2 are the same as in the polymeric and 32-atom LJ fluids discussed above. We note that the T dependence of q_p^2 for the polymeric fluids under constant density conditions is more complicated than for atomic fluids, so we avoid discussing this rarely encountered physical condition in the present paper.

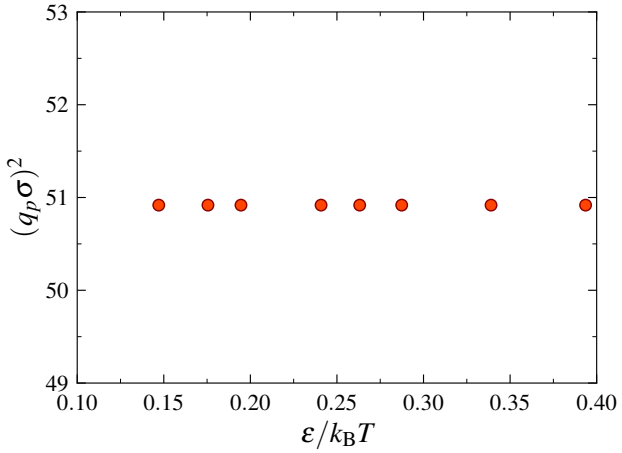

Fig. S4 Mean squared interparticle spacing q_p^2 as a function of $1/T$ for the 32-atom LJ fluid at the density of $\rho = 1.0\sigma^{-3}$.

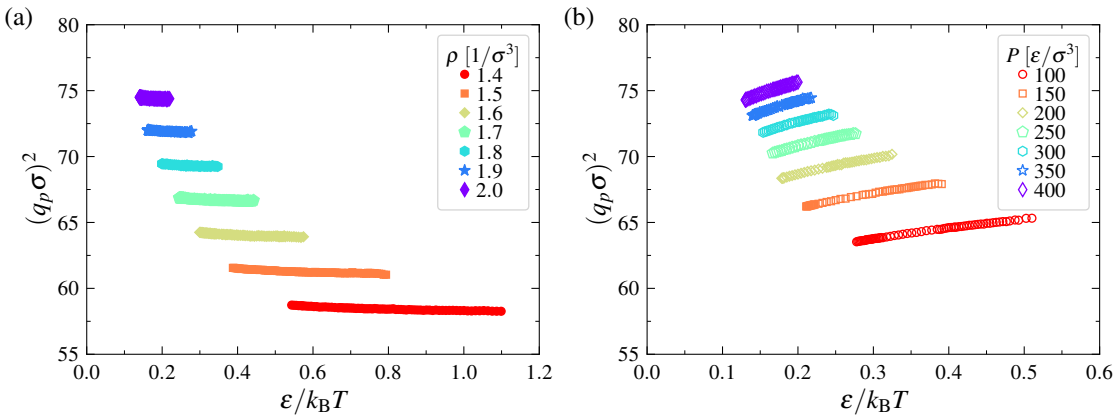

Fig. S5 Mean squared interparticle spacing q_p^2 as a function of $1/T$ for the A particles of the Kob-Andersen fluid. Panels (a) and (b) correspond to the results for fixed ρ and P conditions, respectively.

S2 Relation Between the Non-Ergodicity and Debye-Waller Parameters: A Quantitative Measure of Ergodicity

In the weak ergodicity regime, the dynamics of the material is not strongly chaotic, and the initial fast β-relaxation observed in the self-intermediate scattering function $F_s(q,t)$, driven by the chaotic degrees of freedom, is followed by a metastable non-ergodic state associated with emergent integrable degrees of freedom or "regular motions" in the dynamical system that can persist for a much longer time than the initial fast β-relaxation time, $\tau_{f\beta}$. The relaxation time of the secondary relaxation or α-relaxation time, τ_α, governs the ultimate equilibration time of the system and the relative amplitude of the α-relaxation process defines the "non-ergodicity" parameter, f_{s,q^*}, where the common assumption of taking q_p equal to a constant q^* is adopted for simplicity. Correspondingly, the amplitude of the fast β-relaxation process, $1-f_{s,q^*}$, defines a measure of the degree of ergodicity of the material system. The "non-ergodicity" parameter plays a large role in the modeling of the boson peak in GF liquids and heated crystals.[1]

We show a representative example of the multistep decay of $F_s(q,t)$ for the polymer melt in Fig. S6 based on the approximate expression,[2,3]

$$F_s(q^*,t) = (1-f_{s,q^*})\exp\left[-(t/\tau_{f\beta})^{\beta_f}\right] + f_{s,q^*}\exp\left[-(t/\tau_\alpha)^{\beta_\alpha}\right] \tag{2}$$

where β_f and β_α quantify the non-exponential nature of the fast β- and α-relaxation processes. It is emphasized that Eq. 2 is not justified by any rigorous theory, but this relation provides a good empirical summary of our data, apart from some notable deviations in the intermediate time regime near $t = 1\tau_{\text{ref}}$ at low T. To avoid bias in the fitting of the relaxation times ($\tau_{f\beta}$ and τ_α) and non-exponential index parameters (β_f and β_α) in the fast β- and α-relaxation processes, these relaxation processes are fitted independently.[4] The fitting parameters obtained generally follow the pattern found by Yang et al.[4] In particular, β_f varies in a range between $1\tau_{\text{ref}}$ and $2\tau_{\text{ref}}$ as T is varied, while β_α varies between 0 and 1. The fast β-relaxation time $\tau_{f\beta}$ in molecular fluids increases slowly upon cooling, but this timescale remains on the order of a ps in the T range that we can simulate (see Figs. 7, 17, and 18 in the paper of Yang et al.[4] for

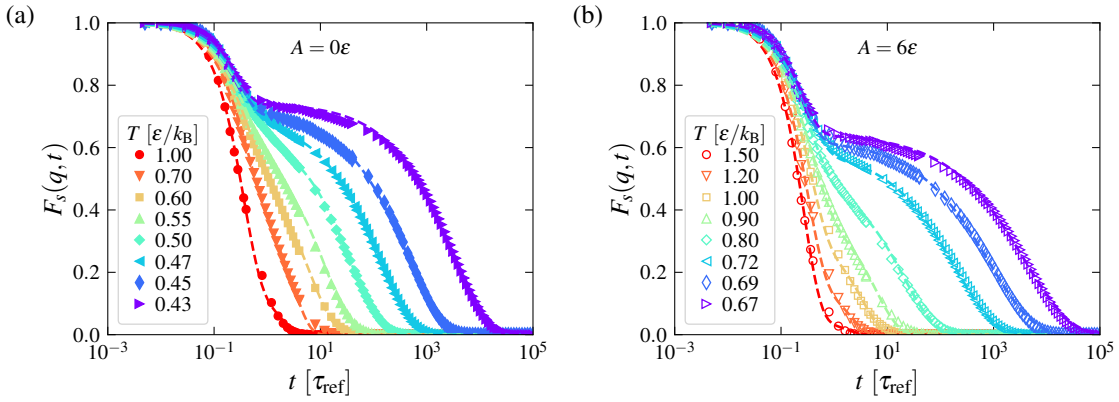

Fig. S6 Self-intermediate scattering function $F_s(q,t)$ of polymer melts for a range of T. Panels (a) and (b) correspond to the results for flexible and semi-flexible polymer melts, respectively. $F_s(q,t)$ exhibits the universal multistep decay of relaxation in glass-forming liquids initiating near the onset temperature T_A, which is well above the glass transition temperature T_g. Lines are the fits to Eq. 2, which serve to guide the eye. The wave number is chosen to be $q = q^* \approx 7.0\sigma^{-1}$, which is close to the first peak position of the static structure factor.

an illustration of this typical behavior). The α-relaxation time τ_α, sharply rises upon cooling, approaching a value near 100 s at the glass transition temperature in experimental systems, a timescale that cannot be reached by MD simulations under quasi-equilibrium conditions.

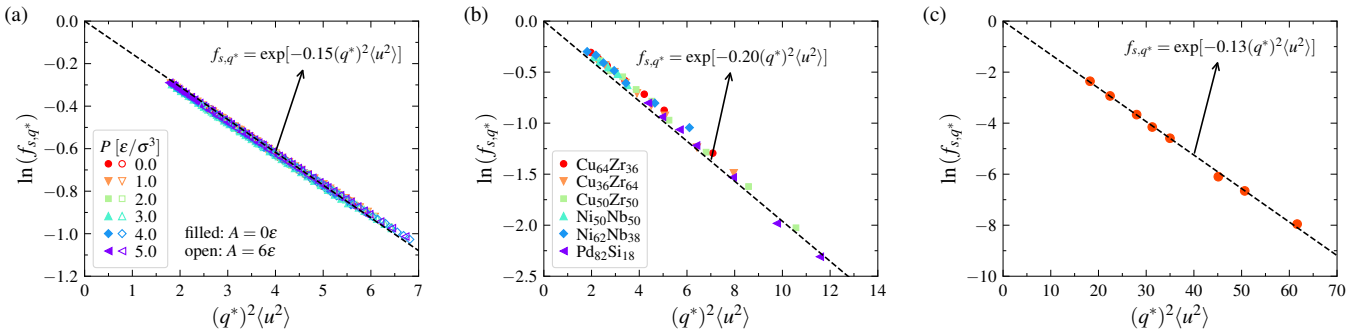

Fig. S7 Relation between the non-ergodicity parameter f_{s,q^*} and the Debye-Waller parameter $\langle u^2\rangle$. Panel (a) shows the results for polymer melts having variable P. Filled and open symbols correspond to the results for flexible and semi-flexible polymer melts, respectively. Panel (b) shows the results for representative metallic glasses. The caging onset time was taken to be $t = 1.5$ ps. Panel (c) shows the results for the 32-atom LJ liquid. Lines show the scaling relations, as indicated in the figure.

We may directly determine the non-ergodicity parameter f_{s,q^*} by fitting the α-relaxation process of $F_s(q,t)$ to the expression, $F_s(q,t) \sim \exp[-(t/\tau_\alpha)^{\beta_\alpha}]$. For generality, we summarize data below for both polymer melts and metallic glasses. f_{s,q^*} is the short-time plateau value of $F_s(q^*,t)$ at the onset of the caging regime, which is a timescale on the order of the fast β-relaxation time. This observation allows us to develop a general approximation of f_{s,q^*} in terms of the "fast dynamics" property, $\langle u^2\rangle$, the mean squared displacement of particles on the caging onset timescale. In the fast β-relaxation regime, the non-Gaussian parameter $\alpha_2(t)$ is generally small in magnitude so that f_{s,q^*} can generally be well described by the Gaussian approximation,

$$f_{s,q^*} \approx \exp\left[-c(q^*)^2\langle u^2\rangle/6\right] \tag{3}$$

where c is a constant. A similar approximation evidently holds for the collective intermediate scattering function.[5] Previous simulation studies on linear and star polymer melts have indicated that Eq. 3 provides an excellent approximation of the simulation estimates of f_{s,q^*} in linear polymer melts having variable stiffness, chain length, and pressure and over a wide range of temperatures, where the interparticle distance parameter q^* was assumed to be constant.[4,6] For illustration, we show f_{s,q^*} for the polymer models studied in the present paper in Fig. S7a, where we find that the relation between f_{s,q^*} and $\langle u^2\rangle$ can be described by Eq. (3) very well.

To further check the universality of the relationship between f_{s,q^*} and $\langle u^2\rangle$, we consider the applicability of Eq. 2 to the simulation estimates of f_{s,q^*} for the metallic glasses and 32-atom LJ fluid studied in the main body of the paper in Fig. S7b and S7c, respectively. Again, the reduction to the form predicted by Eq. 2 is impressive. We also test Eq. 2 against a large body of simulation data for the Kob-Andersen model in Fig. S8a, a model simulated GF liquid, over a wide range of constant density and constant volume conditions.

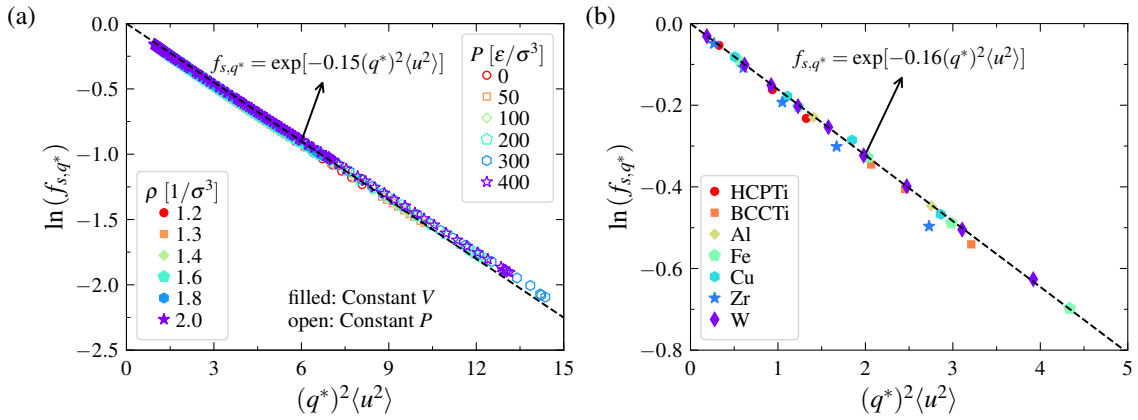

Fig. S8 Relation between the non-ergodicity parameter f_{s,q^*} and the Debye-Waller parameter $\langle u^2\rangle$. Panel (a) shows the results for the binary Kob-Andersen model. Filled and open symbols correspond to the results for constant volume and constant pressure conditions, respectively. Panel (b) shows the results for a series of crystalline metallic materials. The caging onset time was taken to be $t = 1.5$ ps. Lines show the scaling relations, as indicated in the figure.

Finally, we summarize f_{s,q^*} for a range of crystalline metallic materials in Fig. S8b. In each material, we find excellent accord with Eq. 2. We then conclude that the estimated "degree of ergodicity" f_{s,q^*} is a near universal function of $(q^*)^2\langle u^2\rangle$ in a wide variety of liquids.

Parenthetically, we note that all of the data in the present paper are for GF liquids, except for the data shown in Fig. S8b for a range of crystalline metallic materials. These data were taken to check the applicability of Eq. 3 to crystalline materials. MD simulations were employed to investigate various representative crystalline materials studied previously with this relation in view. The materials include models of iron (Fe), tungsten (W), zirconium (Zr), aluminum (Al), copper (Cu), and titanium (Ti). The representative body-centered cubic (BCC) metals (Fe and W) under the thermodynamic conditions of our simulations consist of 13718 atoms, and the representative face-centered cubic (FCC) metals (Cu and Al), the hexagonally packed (HCP) crystals (Zr) consist of 13500 atoms and the Ti crystalline material consists of 32000 atoms.[7] The interaction potentials of all the metals were described using rather standard EAM potentials.[7–11] Each crystal simulation cell was initially relaxed at room temperature (300 K), and then gradually increased temperature (with the heating rate of 1011 K/s) until the model transitioned into a liquid state to obtain binary restart files containing the current simulation state at each temperature of interest. Throughout the heating simulation process, the *NPT* ensemble with zero pressure was utilized, and the dynamic properties of each metal were obtained through an isothermal heating (*NVT*) progress. It is emphasized that all temperatures selected for *NVT* simulations remained below the melting points. Additionally, the periodic boundary conditions were applied, and a time step of 1 fs was used.

References

1 C. Jiang, M. Baggioli and J. F. Douglas, *J. Chem. Phys.*, 2024, **160**, 214505.
2 A. Giuntoli, F. Puosi, D. Leporini, F. W. Starr and J. F. Douglas, *Sci. Adv.*, 2020, **6**, eaaz0777.
3 W. Zhang, J. F. Douglas and F. W. Starr, *J. Chem. Phys.*, 2017, **147**, 044901.
4 Z. Yang, X. Xu, J. F. Douglas and W.-S. Xu, *J. Chem. Phys.*, 2024, **160**, 044503.
5 B. A. P. Betancourt, F. W. Starr and J. F. Douglas, *J. Chem. Phys.*, 2018, **148**, 104508.
6 X. Xu, J. F. Douglas and W.-S. Xu, *Macromolecules*, 2023, **56**, 4929–4951.
7 M. I. Mendelev, T. L. Underwood and G. J. Ackland, *J. Chem. Phys.*, 2016, **145**, 154102.
8 M. I. Mendelev, S. Han, D. J. Srolovitz, G. J. Ackland, D. Y. Sun and M. Asta, *Philos. Mag.*, 2003, **83**, 3977–3994.
9 S. Han, L. A. Zepeda-Ruiz, G. J. Ackland, R. Car and D. J. Srolovitz, *J. Appl. Phys.*, 2003, **93**, 3328–3335.
10 M. I. Mendelev and G. J. Ackland, *Philos. Mag. Lett.*, 2007, **87**, 349–359.
11 Y. Mishin, M. J. Mehl, D. A. Papaconstantopoulos, A. F. Voter and J. D. Kress, *Phys. Rev. B*, 2001, **63**, 224106.